Neurosurg Clin N Am 13 (2002) 313–334

NEUROSURGERY CLINICS OF NORTH AMERICA

Diagnostic imaging for intracerebral hemorrhage

Nafi Aygun, MD*, Thomas J. Masaryk, MD

Diagnostic Radiology, The Cleveland Clinic Foundation, 9500 Euclid Avenue, L10, Cleveland, OH 44195, USA

Intracerebral hemorrhage (ICH) kills more than 20,000 Americans annually and accounts for 10% to 20% of all strokes and two thirds of hemorrhagic strokes [1]. The major causes of ICH are listed as follows:

- Hypertension
- Vascular malformations
  - Arteriovenous malformation (AVM)
  - Cavernous malformation (CM)
- Aneurysm
  - Saccular
  - Mycotic
- Amyloid angiopathy
- Coagulopathy
- Tumor
- Hemorrhagic infarct
- Illicit drug use
- Venous occlusion
- Vasculitis
- Encephalitis

CT remains the diagnostic test of choice in acute ICH because of its exquisite sensitivity to acute hemorrhage, short examination time, low cost, widespread availability, and the technical ease of obtaining a scan in an acutely ill patient. Alternatively, diagnosis of remote hemorrhage may not be possible by CT.

MRI has traditionally been thought to be less sensitive and specific for hyperacute hemorrhage; however, many recent reports have demonstrated increasing promise with sensitivities approaching 100% [2–8]. MRI is a powerful tool for the diagnosis of subacute and chronic hemorrhage because of its great sensitivity and specificity to the byproducts of hemoglobin degradation and, by extension, its ability to estimate the age of a hematoma. In addition, MRI offers a greater potential for identification of preexisting brain lesions [9].

The pathophysiology of ICH is not completely understood [10]. The clinical timing of the actual hemorrhagic event is notoriously inaccurate. The exact time course of hematoma evolution may vary depending on the pathophysiologic state; hence, the staging of ICH is not only arbitrary but is also somewhat inaccurate. To increase the confusion, the pathologic definition of the "same" stage differs from the definition based on imaging findings. With these limitations in mind, those factors that are intrinsic to pathophysiology of the lesion and those known to be relevant to imaging are discussed here.

Biochemical evolution of intracerebral hemorrhage

Hemoglobin is a tetramer of polypeptide chains, with each polypeptide chain having a prosthetic heme group bound within a hydrophobic cleft [11]. Each heme group contains an iron atom in a ferrous (Fe^{2+}) state. The heme iron molecule has six bonds. In the oxyhemoglobin state, which is the predominant state as blood leaves the lungs, there is an oxygen molecule attached to the sixth bond. The interaction of the six bonds with the metal core causes six outer electrons in the five *d* orbitals to pair in the electronic orbitals of the lowest energy. Therefore, there are no unpaired electrons in the oxyhemoglobin state. As blood

* Corresponding author.
E-mail address: aygunn@ccf.org (N. Aygun).

PII: S1042-3680(02)00009-8

travels through the capillaries, oxygen disassociates from hemoglobin because of low partial oxygen pressure in the tissues forming deoxyhemoglobin. In this form, the sixth bond is vacant and there are four unpaired electrons in the five *d* suborbitals. This is a physiologic and reversible process.

When removed from the high oxygen environment of the circulation, the bulk of the blood remains in the oxyhemoglobin state for an additional 2 to 3 hours. There is immediate activation of the clotting cascade with incorporation of other cellular elements to the red blood cells (RBCs) in the formation of a clot. As the clot matrix forms, soluble plasma proteins are converted to a gel matrix, which is then concentrated more by platelet contraction. Evaluation of a retracted clot demonstrates a hematocrit of approximately 90%. During retraction, some of the serum is released to the periphery. In the meantime, deoxyhemoglobin forms at the periphery of the hematoma followed by the failure of the metabolic pathways (methemoglobin reductase systems) that prevent oxidation of heme iron, leading to oxidative denaturation of hemoglobin to methemoglobin. In methemoglobin, heme iron is in a ferric (Fe^{3+}) state with five unpaired *d* electrons and is unable to bind oxygen. Conversion of hemoglobin to methemoglobin is a reversible reaction, which requires the presence of some oxygen to take place, although not all the factors affecting this process have been described [12,13]. ICH leads to the most rapid transition from one stage to the other owing to the ideal partial oxygen pressure in the brain parenchyma (~20 mm Hg) for oxidative denaturation of hemoglobin [14]. Higher oxygen concentrations (~40 mm Hg) in the subdural, epidural, subarachnoid, and intraventricular compartments result in slow progression of hemoglobin evolution.

As part of the response of brain microvasculature to hematoma, sprouts of endothelial cells begin growing on approximately the third day. By 1 week, these form a lumen and carry circulating blood to the margins of the hematoma. With concurrent oxidative denaturation of methemoglobin, heme proteins are formed. These are phagocytosed by macrophages and glial cells, and the iron is stored in ferritin to be transported to the reticuloendothelial system for recycling. Excess iron is stored as hemosiderin.

MRI of intracerebral hemorrhage

The MRI appearance of ICH is an evolving pattern of variable signal intensities that depends on the various oxygenation states of hemoglobin and hemoglobin byproducts present. This evolution is rather predictable, although variations exist. Several other factors, including location of the hematoma, operating field strength, mode of image acquisition, status of the RBCs, presence of underlying brain lesion, and coagulopathy influence the MRI appearance. Basic understanding of the biochemical evolution of ICH and magnetic properties of matter that affect the MRI signal is necessary to interpret the MRI of ICH.

Magnetic properties of hemoglobin byproducts

A complete discussion of image generation in MRI is beyond the scope of this article, and interested readers are referred to other resources [15,16].

A magnetic field is generated by a moving electric charge. The strength of the magnetic field is determined by the size and momentum of the electric charge. The magnetic field generated by the unit charge is called a magnetic dipole. An electron in an atomic orbital represents a moving charge with orbital angular and spin angular momentum that generates a magnetic field. Although nuclear magnetic interactions occur and nuclear magnetization (primarily of protons) is the basis of the generation of the MRI signal, the magnetic properties of tissue are mainly determined by the electronic configuration of the atoms and molecules [17]. Unpaired electrons produce a magnetic dipole as a result of their spin angular momentum; the greater the number of unpaired electrons, the greater is the created magnetic dipole. The interaction between the electronic dipole of the unpaired electrons and the nuclear dipole of the proton is termed *dipole–dipole interaction* and has a profound effect on T1 and T2 shortening when these electronic magnetic moments correctly orient and fluctuate at or near the MRI signal (Larmor) frequency for protons. Substances that have no intrinsic magnetic field but shorten either T1 or T2 when placed in a magnetic field are termed *paramagnetic.* Because the T1 time of biologic substances is generally 5 to 10 times longer than the T2 time, discernible T1 shortening occurs at much lower concentrations of paramagnetic substances [18]. T1 shortening results in bright signal on T1-weighted images (T1WIs).

Three criteria need to be fulfilled for T1 shortening to occur: (1) a paramagnetic substance must be present, (2) the electron spin relaxation time must be long enough to enhance effective relaxation of water protons, and (3) the hydrogen atom of the water molecule must be able to approach

the paramagnetic center (heme iron) within 0.3 nm. Despite the moderately strong paramagnetism of deoxyhemoglobin, T1 shortening is not observed in its presence, because dipole–dipole interactions cannot take place owing to shielding of heme iron from the close approach of water molecules. Conversely, strongly paramagnetic methemoglobin demonstrates marked T1 shortening, because the change in the molecular conformation of hemoglobin in the methemoglobin state allows protons to approach the heme iron. Again, because of the molecular conformation of methemoglobin, the electron spin relaxation time is closer to the Larmor frequency for water protons, resulting in more effective relaxation [18].

For paramagnetic substances in aqueous solutions, T1 shortening dominates the T2 shortening in concentrations usually encountered. Another paramagnetic mechanism known as *magnetic susceptibility effect* can selectively shorten T2 without affecting T1, however [19]. Paramagnetic substances with unpaired electrons produce local magnetic nonuniformity, which leads to dephasing and thus to T2 shortening. The greater the nonuniformity, the greater is the T2 signal decrease. Because the nonuniformity is proportional to the magnetic field strength, the signal decrease is greater at higher field magnets.

An additional magnetic susceptibility effect related to a field strength–dependent phenomenon (which accounts for the loss of T2 signal) is the dephasing of spins caused by diffusion of water molecules across intact RBC membranes when intracellular deoxyhemoglobin or methemoglobin is present. In this state, the induced magnetic field within RBCs is greater than the nonparamagnetic extracellular plasma such that the diffusing water molecules experience a magnetic gradient, resulting in T2 signal decrease. Magnetic susceptibility effects account for a substantial portion of the observed T2 shortening related to deoxyhemoglobin and intracellular methemoglobin at high-field magnets.

Clark et al [20] demonstrated that polymerization of fibrinogen to form fibrin and retraction of fibrin clot by platelets lead to a 17% reduction in T2 at 2.1 T. Because T2 shortening as a result of clot retraction is not dependent on field strength, a larger contribution to signal loss from these effects is expected at lower magnetic field strengths. This may lead to somewhat delayed detection of T2 shortening in low-field magnets, particularly in those patients who have coagulopathy. The same authors also demonstrated that increasing the hematocrit increases T2 shortening in a linear fashion and that this effect increases with increasing field strength.

Temporal evolution of intraparenchymal hemorrhage defined by MRI

Most parenchymal hematomas evolve in a predictable fashion, although variations exist (Table 1). The exact time course of biochemical changes may vary depending on the precipitating pathophysiologic state. The MRI appearance is influenced by the acquisition mode and field strength [13]. Five stages of hemorrhage can be identified by MRI. Although it is practical to describe the evolution of a hematoma in these well-defined stages, they frequently coexist. By convention, the stage of the hematoma is defined by the most mature form of hemoglobin present. In this discussion, all images are acquired at 1.5 T.

Hyperacute hematoma

Freshly extravasated blood consists of intact RBCs with oxyhemoglobin, plasma, and other cellular elements. Because there is no paramagnetic substance at this time, there can be no T1 or T2 shortening. The MRI appearance of hyperacute

Table 1
Evolution of hemoglobin byproducts

				Signal intensity compared to gray matter	
Hematoma stage	Time	Hemoglobin state	Compartment	T1WI	T2WI
Hyperacute	0–24 hours	Oxyhemoglobin	Intracellular	=to ↓	↑↑
Acute	Several hours to 3 days	Deoxyhemoglobin	Intracellular	↓↓	↓↓↓
Subacute early	3–7 days	Methemoglobin	Intracellular	↑↑↑	↓↓↓
Subacute late	7–14 days	Methemoglobin	Extracellular	↑↑↑	↑↑↑
Chronic	14+ days	Hemosiderin	Intracellular	↓	↓↓↓

T1WI = T1-weighted image; T2WI = T2-weighted image.

hemorrhage is essentially identical to that of many brain lesions in the first 3 hours (ie, isointense to slightly hypointense T1 signal and hyperintense T2 signal). Shortly after ictus, deoxyhemoglobin starts to form at the periphery of the hematoma as a result of favorable partial oxygen tension for hemoglobin–oxygen disassociation in the surrounding brain parenchyma. Conversion to deoxyhemoglobin continues in the ensuing hours. At approximately 24 hours, deoxyhemoglobin becomes the dominant byproduct within the hematoma. The minimum amount of deoxyhemoglobin needed for visible T2 signal change depends on the field strength and imaging technique [19]. After the first few hours, a thin rim of decreased T2 signal is observed around most hematomas, particularly at high-field magnets (Fig. 1).

Hyperacute hemorrhage is rare in clinical practice, because at least several hours pass between the ictus and MRI acquisition in most situations.

Acute hematoma

Approximately 1 to 3 days after the ictus, most of the hematoma has been converted to paramagnetic deoxyhemoglobin, which is shielded from the nonparamagnetic extracellular environment by the intact RBC membrane. Diffusing water molecules across the RBC membrane experience a magnetic gradient that results in local field nonuniformity and T2 signal decrease. At this stage, virtually the entire hematoma is markedly hypointense on T2-weighted images (T2WIs) (Figs. 2–4). There is usually a surrounding area of hyperintensity reflecting vasogenic edema and extracted serum.

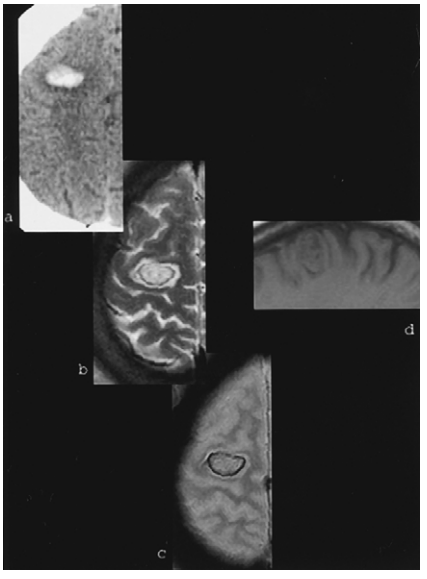

Fig. 1. (a) Acute lobar hemorrhage in a patient with history of cocaine abuse. The only clue to the acute hematoma on MRI is the hypointense rim on the T2-weighted image as a result of deoxyhemoglobin formation at the periphery (b), which is much better depicted on the gradient-echo image (c). The lesion is barely perceptible on the T1-weighted image (d).

Despite the paramagnetic property of deoxyhemoglobin, no T1 shortening is seen in the acute phase, because the molecular configuration of deoxyhemoglobin does not allow water molecules to approach the heme iron. The observed mild hypointensity on the T1WI is a reflection of the short T2 of deoxyhemoglobin.

It should be noted that under low-field conditions, acute hematoma is essentially isointense to brain parenchyma on conventional spin-echo (CSE) T2WIs. Utilization of a long TR as well as a long TE may improve the detection of hematoma on T2WIs. Gradient-echo (GRE) imaging is also useful for this purpose in low-field systems [21].

Subacute hematoma

In the early subacute stage, deoxyhemoglobin is oxidized to methemoglobin at the periphery of the hematoma as a result of favorable oxygen tension in the surrounding brain parenchyma. Because methemoglobin is paramagnetic, a high-intensity rim appears on T1WIs beginning approximately 2 to 3 days after the ictus and converges radially inward during the following days. Hematoma continues to be markedly hypointense on T2WIs in the early subacute phase because of the paramagnetic methemoglobin as well as the magnetic gradient created across the RBC membrane (Fig. 5).

Impaired cellular mechanisms lead to loss of cellular integrity approximately 7 days after the hemorrhage, resulting in loss of T2 shortening effects from compartmentalized methemoglobin. T1 signal continues to be high and dominates the late subacute phase. T2WIs also demonstrate a high signal hematoma despite the paramagnetic methemoglobin (Figs. 2 and 6). This seemingly contradictory situation results mainly from the prominent T1 shortening and relatively high concentrations of proteins within the hematoma increasing the proton density and T2 signal [22].

Chronic hematoma

The appearance of a dark rim around the hematoma defines the chronicity at around the day 14.

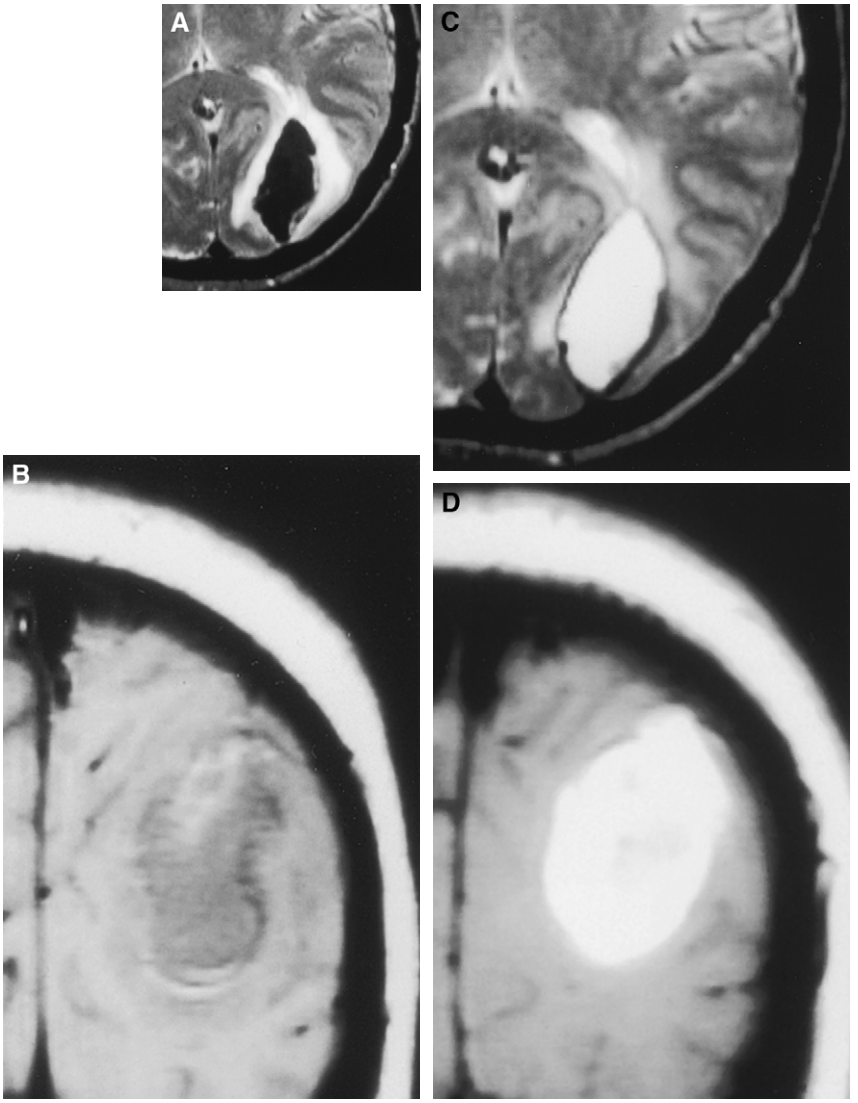

Fig. 2. MRI studies obtained 36 hours and 10 days after the clinical event. (A,B) Acute left occipital hematoma. Note decreased T2 (A) and T1 (B) signals in the center of the hematoma as a result of deoxyhemoglobin. A small amount of intracellular methemoglobin has already formed at the periphery. Surrounding increased signal on a T2-weighted image (T2WI) reflects vasogenic edema and extracted serum. In the late subacute stage, the hematoma demonstrates markedly increased signal on both a T2WI (C) and a T1-weighted image (D) because of extracellular methemoglobin.

This is caused by ferritin and hemosiderin deposition in the macrophages and glial cells and is apparent on T2WIs because of magnetic susceptibility effect [23,24]. Although these iron storage products are paramagnetic at physiologic temperatures, they are inaccessible to water molecules; thus, no dipole–dipole interaction takes place. Because extracellular methemoglobin is still present, however, there continues to be an increased T1 signal in the center of the hematoma, which decreases gradually but persists for several months after the bleed. Occasionally, methemoglobin may remain for years, but the presence of methemoglobin in an area of remote hemorrhage generally suggests rehemorrhage or an underlying lesion, leading to abnormal evolution [25]. The dark rim seen on T2WIs thickens as ferritin/hemosiderin accumulates. This area of marked hypointensity

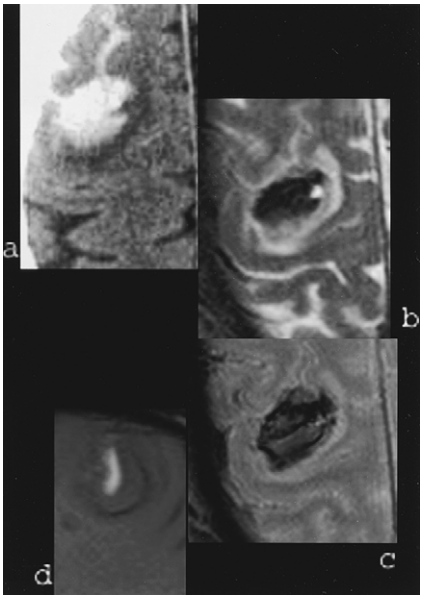

Fig. 3. Hypertensive lobar hemorrhage. (a) Small right frontal hematoma with a small amount of subarachnoid hemorrhage on CT. (b) A T2-weighted image (T2WI) shows markedly decreased signal, reflecting deoxyhemoglobin and thus acute hematoma. (c) Note that the hematoma appears larger on the gradient-echo image because of increased susceptibility effect. A small area of increased signal on a T1-weighted image at the periphery of the hematoma is caused by methemoglobin, which is intracellular, because there is no corresponding high signal on the T2WI (d).

remains indefinitely in most hematomas (Figs. 7 and 8).

It has been well established that MRI is quite sensitive for the detection of subacute and chronic ICH. It is also known that GRE sequences, particularly those with a low flip angle and long echo time, are more sensitive than CSE and fast-SE sequences (Figs. 9 and 10) [26,27]. GRE sequences were found to be superior to diffusion-weighted echoplanar images as well [28,29]. Despite the theoretic advantages of CSE, there is no clinically significant difference demonstrated between CSE and fast-SE [30]. Recently, a number of experimental and clinical studies reported high sensitivity for detection of hyperacute ICH [2–8]. As a reflection of the difficulties in performing an early MRI scan on these patients, studies included limited numbers of patients. Nevertheless, there is convincing evidence that MRI can detect ICH as early as 2.5 hours with a high sensitivity using GRE sequences. Caution must be exercised, however, because most

Fig. 4. Small acute hematoma in the left parietal subcortical white matter caused by aspergillus infection. The markedly decreased signal on this T2-weighted image is secondary to deoxyhemoglobin, which is difficult to differentiate from hemosiderin without a T1-weighted image. The vasogenic edema is a clue to the acute nature of the lesion.

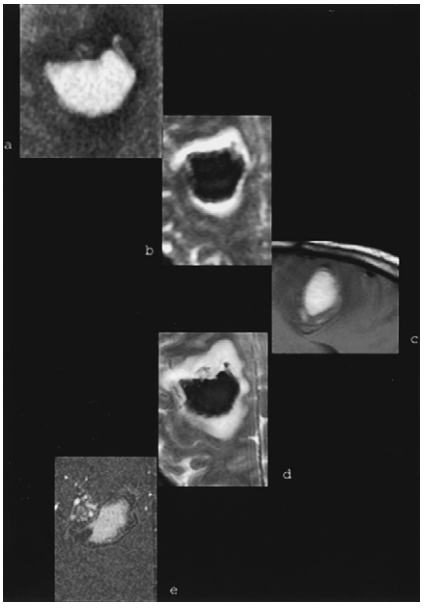

Fig. 5. (a) Acute hematoma on CT. On follow-up MRI, the markedly decreased signal on the diffusion-weighted (b) and T2-weighted (d) images and the increased signal on the T1-weighted image (c) are secondary to intracellular methemoglobin. Individual partition from a Magnetic Resonance Angiography (MRA) uncovers the underlying arteriovenous malformation.

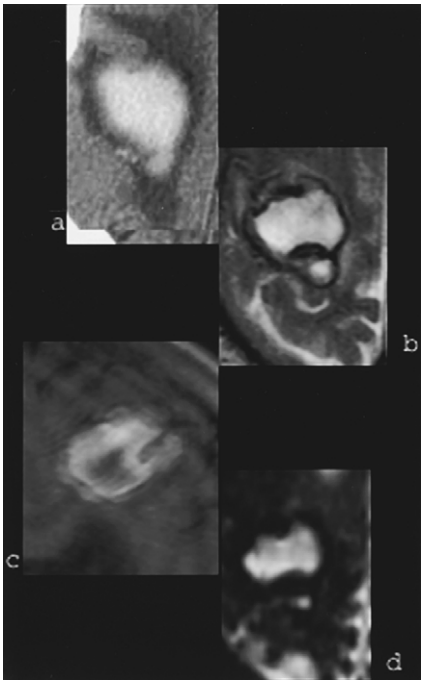

Fig. 6. Hypertensive lobar hemorrhage. (a) Acute hematoma in the right frontal lobe. High signal on the T1-weighted image (TIWI) and T2-weighted image (T2WI) obtained 10 days later indicates extracellular methemoglobin. A hemosiderin rim has already formed (b) and is better seen on the diffusion-weighted image (d). Note that hyperacute and late subacute hemorrhage may be identical on the T2WI, emphasizing the importance of evaluating both the T1WI and T2WI together (compare with Fig. 1).

of the patients in the reported series had rather large hematomas, making the diagnosis easy. The evaluation of the peripheral brain may be limited as a result of susceptibility artifacts arising from the skull on GRE imaging, which is the most sensitive pulse sequence. Furthermore, the specificity of MRI may be limited in the hyperacute stage [31]. Therefore, it is premature to conclude that MRI can replace CT in the hyperacute stage.

CT of intracerebral hemorrhage

Acute hemorrhage is seen as increased attenuation on CT. This increased attenuation is related to the high electron density of the protein (globin) component of the hemoglobin molecule [32]. The CT attenuation value of whole nonclotted blood

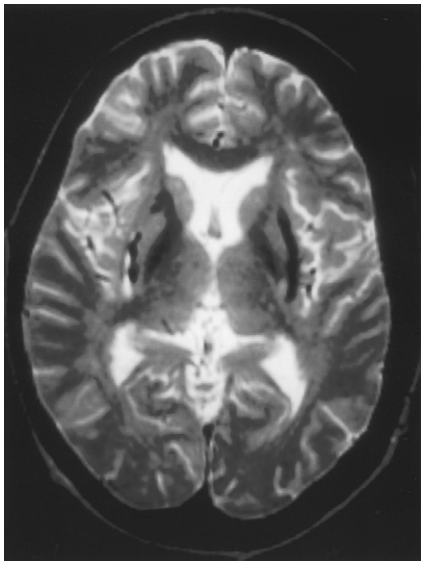

Fig. 7. Bilateral curvilinear areas of decreased signal in the putamina reflecting remote hemorrhages in this patient with hypertension.

with a hematocrit of 45% is 56 Hounsfield units (HU), and that of the cerebral cortex is 37 to 40 HU [32,33]. A few hours after acute hemorrhage, the hematocrit is measured at 90% as a result of clot retraction, which continues to occur in the first

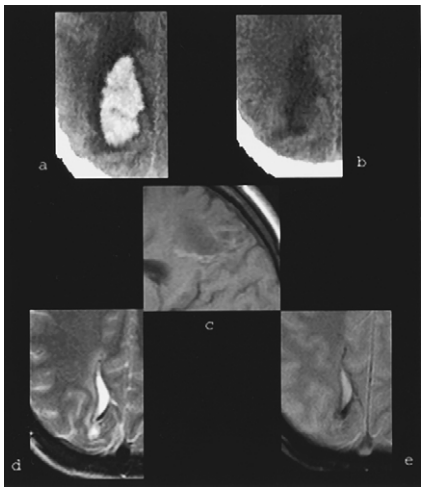

Fig. 8. (a) Acute right parietal white matter hematoma caused by an underlying arteriovenous malformation. (b) Follow-up CT shows no sign of hemorrhage. A fluid-filled cavity is seen on MRI with a hemosiderin rim on the T2-weighted (d) and gradient-echo (c) images, consistent with chronic hematoma. (c) A small amount of methemoglobin persists on the T1-weighted image.

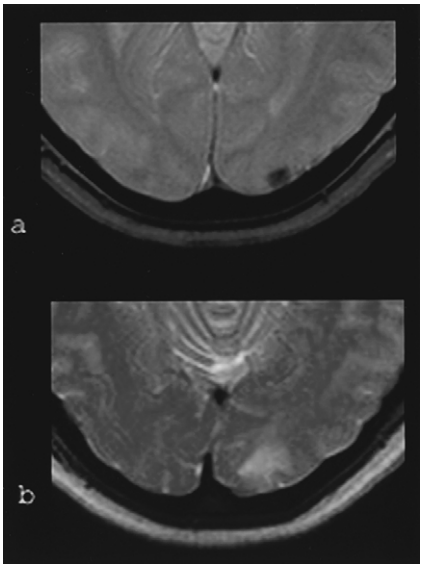

Fig. 9. Central nervous system vasculitis. Small hemorrhagic lesion in the left occipital cortex/subcortical region. Note that it is difficult to recognize the hemorrhagic nature of the lesion on the fast spin-echo T2-weighted image (b) without the gradient-echo image (a).

days, leading to increasing attenuation values of the hematoma up to 3 days [33]. At this time, the attenuation of acute hematoma is 80 to 86 HU. There is usually a halo of decreased attenuation around the sharply demarcated acute hematoma, reflecting a combination of edema and extracted serum.

Relatively less increased attenuation can be observed in acute hematomas in patients who have coagulopathy as a result of impaired clot formation and/or retraction. Another factor that may affect the attenuation of hematoma is the hematocrit of the patient. Hemorrhage into a preexisting lesion may result in dilution of blood byproducts. Presence of fluid–fluid levels in the hematoma suggests an underlying coagulopathy or hemorrhage into a preexisting cavity [34].

Independent of the etiology of hemorrhage, an enhancing rim is observed on contrast-enhanced scans in the subacute stage, reflecting disruption of the blood–brain barrier and "leaky" neovascularity [35,36].

In the following days, the attenuation of the hematoma decreases at a rate of 1.5 HU/d [37]. In the subacute stage, a slightly hazy margin can be observed. Approximately 3 weeks after ictus, an intraparenchymal hematoma is similar in attenuation to the adjacent normal brain. Resolution of mass effect generally lags behind the normalization of attenuation, however (Fig. 11).

In the early chronic stage, a hematoma appears as an ill-defined low-attenuation area. An area of cerebrospinal fluid–like attenuation with local volume loss is seen in the chronic phase. Because there is no blood byproduct seen on CT in the chronic stage, the diagnosis of hemorrhage is inferential.

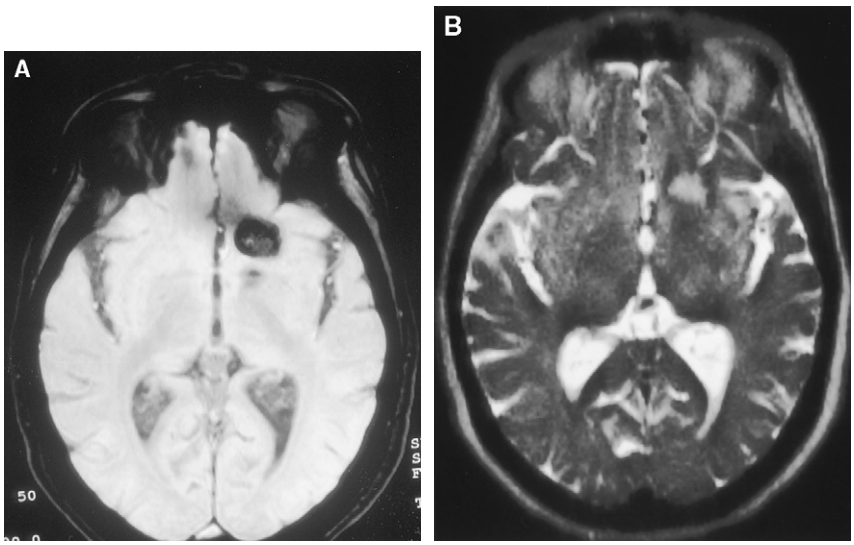

Fig. 10. Cavernous malformation (CM). (a) There are two lesions in the left frontal lobe and internal capsule with hemosiderin rings, compatible with CMs on the gradient-echo image. Note that on the fast spin-echo T2-weighted image, the smaller CM is not seen and it is impossible to identify the hemosiderin deposition associated with the larger CM.

Fig. 11. Lobar hemorrhage. Left occipital hematoma on CT studies obtained 2 (a), 10 (b), 13 (c), 28 (d), and 40 (e) days after ictus. Note that despite the gradual decrease in attenuation, mass effect persists. Peripheral contrast enhancement is seen on the study performed on day 17 (f).

Etiology of intracerebral hemorrhage

Hypertensive intracerebral hemorrhage

Seventy percent to 90% of the patients who present with acute ICH have elevated blood pressure [1,38,39]. Increased blood pressure, however, may be secondary to increased intracranial pressure and the resulting Cushing's reflex. In one study, only 45% of the patients with acute ICH had a history of hypertension [40]. In another study, 48% of the thalamic, putaminal, or posterior fossa hematomas and 65% of the lobar hematomas were associated with an underlying structural lesion in patients who were younger than 45 years of age and did not have preexisting hypertension [41]. Therefore, it is important to evaluate the patient's age and previous history along with imaging findings before making a presumptive diagnosis of ''hypertensive ICH'' [40]. One must also be aware of the prognostic implications of ICH unrelated to hypertension.

Hypertensive ICH is believed to occur as a result of rupture of microaneurysms involving the penetrating vessels [42]. Hematoma enlargement from continuing bleeding is associated with clinical deterioration, and it is not uncommon for such enlargement to occur in the first hours after ictus [43–45]. Heavy drinking, decreased level of consciousness at presentation, irregularly shaped hematomas, and low level of fibrinogen are associated with a greater likelihood of hematoma enlargement [45, 46]. Enlargement of a hematoma can reliably be identified with CT when it is greater than 12.5 cm^3 or greater than 140% of its original size [47]. Increasing mass effect is invariably associated with enlargement of a hematoma in the first few days after ictus. There is a second time point in the second or third week of evolution of the hematoma when an increase in mass effect is observed because of enlargement of the perihematoma edema [48]. This is generally not associated with clinical deterioration, however, and may be related to absorption pathways of the edema fluid [49].

The typical locations of a hematoma caused by hypertensive ICH are the putamen, caudate, thalamus, lobe of a hemisphere, cerebellum, and pons (Fig. 12).

The putamen is the most common location for hypertensive ICH. The hematoma may be localized to the anterior, middle, or posterior putamen. The resultant neurologic syndrome and patient's outcome may be different for different locations. Expanding putaminal hematomas can involve the anterior limb of the internal capsule, globus pallidus, and caudate medially; the insular region laterally; and the posterior limb of the internal capsule dorsally. Intraventricular rupture is not uncommon.

Lobar hemorrhages typically occur at the gray–white matter junction in the subcortical region.

Thalamic hemorrhages may involve the lateral or medial thalamus (Fig. 13). Medially expanding hematomas rupture into the third ventricle. The posterior limb of the internal capsule is often involved with lateral extension.

Pontine hemorrhages are often devastating events. They involve the junction between the basis pontis and tegmentum in the midpons.

Cerebellar hematomas are usually located in the region of the dentate nucleus. Because of their critical location, they generally require emergent surgery.

Caudate hematomas either expand medially to rupture in the ventricle or dissect posterolaterally or posteroinferiorly. Caudate hematomas with posterolateral extension may be indistinguishable from putaminal hematomas.

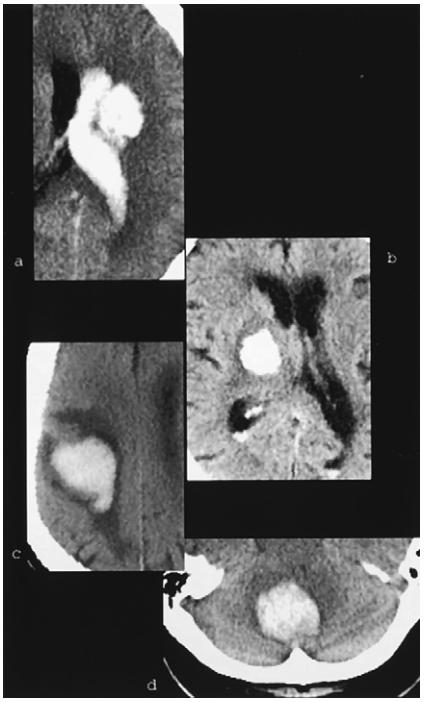

Fig. 12. Common locations of hypertensive hemorrhage. Left putaminal with intraventricular extension (a), right thalamic (b), lobar (c), and cerebellar (d) hematomata in different patients.

Clinically silent remote microbleeds and ischemic lesions are not infrequently observed in patients with hypertensive ICH (Fig. 14) [50–52].

Intraventricular rupture of a parenchymal hematoma carries a worse prognosis. Intraventricular hemorrhage (IVH) in the absence of a parenchymal hemorrhage is rare. Etiologies of isolated IVH include aneurysms, vascular malformations, and coagulopathies [53,54]. The role of hypertension as the primary causative factor is not clear, although hypertension is not uncommonly associated with isolated IVH [55,56].

Hematomas larger than 40 cm^3 are associated with a worse prognosis [57]. The hematoma volume can be accurately estimated by multiplying the greatest dimensions of the hematoma and dividing the result by 2 [58].

The overall mortality of ICH is the highest among various types of stroke and approaches 60%, which has been relatively constant despite refinements in patient care. Intraventricular rupture, low Glasgow Coma Scale scores at presentation, large hematomas, and hydrocephalus are the major predictors of poor outcome [57,59–61].

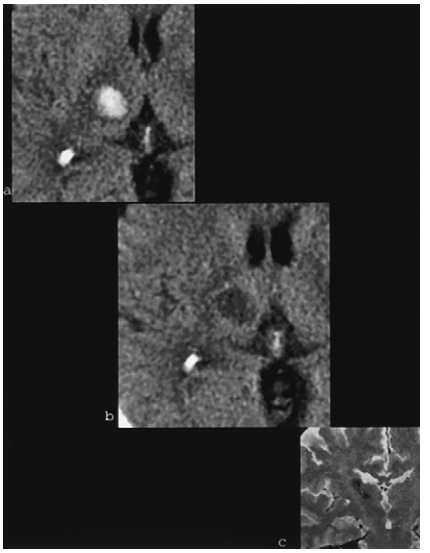

Fig. 13. Hypertensive hemorrhage. (a) Small acute hematoma in the right thalamus. (b) A well-defined area of decreased attenuation in the thalamus on CT obtained 23 days after ictus is difficult to identify as evolving hematoma without the previous study. (c) More than a year later, T2-weighted MRI demonstrates a linear hemosiderin deposition.

There is no standard treatment (medical or surgical) for hypertensive ICH [62]. The discouraging results of early randomized trials investigating the efficacy of surgery have led to great variability in treating this deadly disease [63,64]. With the recent advances in less invasive surgical methods, there is now a growing interest in the surgical management of hypertensive ICH. More recent randomized trials have demonstrated a trend for surgery to reduce the mortality and morbidity, although there is still need for a large randomized trial that has the statistical power to achieve the necessary high level of accuracy [65]. Zuccarello et al [66] compared the 3-month outcome for urgent surgical evaluation and nonsurgical management of ICH and demonstrated that a large randomized trial is feasible. Montes et al [67] and Miller et al [68] reported encouraging preliminary results regarding their experience with aspiration of ICH under stereotactic CT guidance after thrombolysis. There is currently a multicenter randomized trial underway [69].

The rationale of early surgical hematoma evacuation is based on the concept that there is a penumbra of functionally impaired but salvageable brain tissue surrounding the hematoma. Animal models of ICH have demonstrated that there

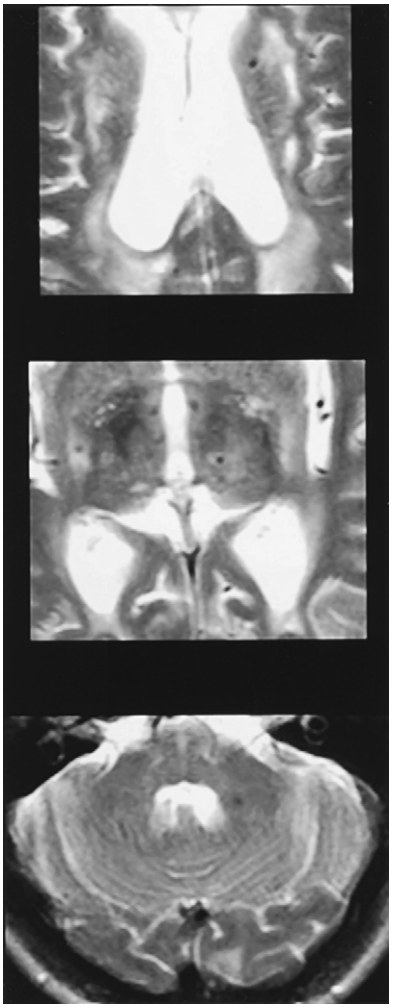

Fig. 14. Hypertensive microhemorrhage. Punctate areas of decreased signal on the T2-weighted image in the putamina bilaterally, left thalamus, and left cerebellum, reflecting remote microhemorrhages in this hypertensive patient.

is increased mass effect and edema with decreased perfusion around the hematoma and that the development of these can be prevented with early hematoma evacuation [70]. Qureshi et al [71] analyzed the injured, necrotic, and apoptotic cells around iatrogenically created hematomas in rabbits and demonstrated potentially salvageable brain tissue. Siddique et al [72] showed improved regional perfusion after hematoma evacuation in human patients, although the role of decreased perfusion in the pathogenesis of brain damage is not clearly understood [73]. Using positron emission tomography, despite the presence of hypoperfusion, no increase in oxygen extraction fraction was observed in the region of hypoperfusion (suggesting a factor other than ischemia as the cause of brain damage in ICH) [74]. Hall et al [75] presented evidence that oxidation of hemoglobin may account for the development of edema and brain damage. As the pathogenesis of brain damage is being elucidated, what imaging can offer to help in this process remains to be seen. Tissue perfusion can be reliably measured with positron emission tomography, single photon emission computed tomography, and CT, and these modalities may separate the patients who are likely to benefit from surgery from those who are not if decreased perfusion is proved to be the causative factor for brain injury in ICH. Unfortunately, susceptibility-related artifacts hinder the evaluation of the brain parenchyma in the vicinity of the hematoma with powerful tools of modern neuroimaging, such as perfusion–diffusion MRI and magnetic resonance spectroscopy, although some authors have reported encouraging results [76].

Cerebral amyloid angiopathy

Cerebral amyloid angiopathy (CAA) is characterized by deposition of amyloid in the cortical and leptomeningeal vessels and is a major cause of ICH, particularly in the normotensive elderly [77]. The apolipoprotein E ε2 and ε4 alleles are associated with CAA, earlier age at first hemorrhage, and increased risk of recurrent hemorrhage, but they are neither specific nor sensitive for CAA [78,79]. The specificity and sensitivity of brain biopsy are not high because of the frequent presence of CAA in healthy individuals and patchy involvement of the brain with CAA [80,81]. The clinical hallmark is recurrent lobar hemorrhages, but CAA may present with recurrent transient neurologic symptoms and progressive dementia [82]. The first hemorrhage may be indistinguishable from hypertensive ICH on imaging studies. Demonstration of previous hemorrhages in a lobar location has been proven to be helpful in the clinical diagnosis of CAA (Fig. 15). GRE MRI is best suited for this purpose [83]. Approximately 50% of patients develop recurrent hemorrhage in 1.5 years after the first hemorrhage. GRE MRI is a useful tool for assessment of progression.

Arteriovenous malformations

AVMs are congenital vascular abnormalities that develop as a result of failure of regression of

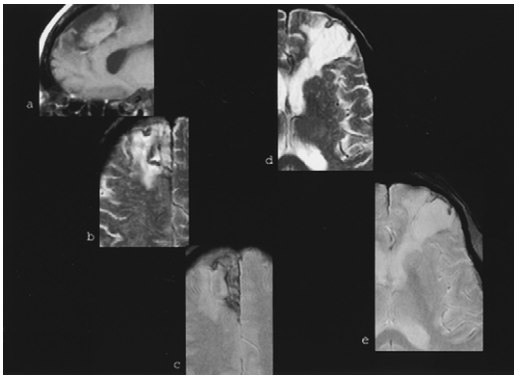

Fig. 15. Amyloid angiopathy. Lobar hemorrhages of different ages in the frontal lobes. (a) High signal on the T1-weighted image because of persistent methemoglobin in the right frontal chronic hematoma 8 months after the event. (d,e) The dark hemosiderin rim around the encephalomalacia in the left frontal lobe is the only evidence of prior hemorrhage. (c,e) Note that hemosiderin is better demonstrated on the gradient-echo images.

the primitive direct communications between the arterial and venous systems, which leads to an arteriovenous connection through a nest of abnormal vessels supplanting the normal capillary bed. The clinical presentation of AVMs is predominantly through intracranial hemorrhage, incapacitating headaches, seizures, and progressive neurologic deficits related to adjacent brain ischemia [84–87]. Larger AVMs are more likely to present with seizures and/or ischemia, whereas smaller AVMs more often hemorrhage [88].

The natural history of untreated AVMs is associated with an annual rate of hemorrhage estimated to be 2% to 4% [88–94]. In addition, the mortality from an unruptured AVM is approximately 1% per year, and the mortality associated with the first hemorrhage is approximately 10%. AVM characteristics that predispose to future hemorrhage include central venous drainage, periventricular location, and intranidal aneurysm.

Identification of enhancing serpentine structures on CT and flow voids on MRI in association with ICH makes the diagnosis of AVM relatively easy. On rare occasions, enlarged internal cerebral veins or the vein of Galen may be the only clue to a small AVM. Imaging evidence of remote hemorrhage is not uncommon even when there is no clinical history of prior hemorrhage.

Cavernous malformations

CMs appear as well-circumscribed multilobulated masses filled with blood on gross inspection and consist of abnormal thin-walled vascular caverns with no intervening brain parenchyma on histopathologic examination. A variably thick zone of gliotic and hemosiderin-stained brain tissue surrounds the CM. Calcification or ossification is common. The prevalence of CMs has apparently increased with the liberal use of MRI and ranges between 0.45% and 0.90% [95]. A pattern of familial clustering and frequency of multiple lesions in the familial cases have been recognized [96]. Recently, a founder mutation on chromosome 7q (CCM1 gene) and several other point mutations have been demonstrated to be responsible for the development of CMs [97–99]. The mutations predicted truncation of the Krit1 mRNA encoded by CCM1, supporting the contention that a CM results from loss of Krit1 protein function and the possibility that this protein acts as a tumor suppressor [100,101].

The presence of immature or new blood vessels and expression of vascular endothelial growth factor within CMs demonstrated by immunohistochemical studies support the hypothesis that CMs develop de novo and that angiogenic proliferation may be responsible for the CM growth [102–104]. A number of studies attempted to determine the natural course of CM utilizing serial MRI scans and demonstrated that they change in size, number, and imaging features, suggesting repeated hemorrhages over time [105–107].

A large number of CMs are asymptomatic and first noted on MRI or CT scans performed for unrelated reasons. Focal seizure activity is the most common symptom associated with CMs, followed by focal neurologic symptoms, which are likely the result of local irritative effects of hemosiderin, gliosis, and intralesional or extralesional hemorrhage. Chronic headache is a less common presenting symptom. Acute headache caused by overt hemorrhage does occur but is rare.

CMs are the most common "angiographically occult" vascular malformation of the brain. They occur throughout the brain but are more common in the subcortical white matter in the supratentorial compartment and in the pons in the infratentorial compartment. Rare cases of leptomeningeal or dural CMs as well as giant cystic CMs have been reported [108].

On unenhanced CT, a rounded isoattenuating to hyperattenuating mass is seen. Calcification is

common. A slight mass effect may be present. Enhancement is variable.

The MRI appearance is characteristic and consists of a central area of increased signal with mottled areas of low signal on the T1WI and T2WI (extracellular methemoglobin and calcification) and a variably thick rim of markedly decreased signal (hemosiderin and ferritin), which is better seen on T2WIs and GRE images (Figs. 16 and 17). Unless there has been a recent hemorrhage, there is no edema or significant mass effect in the surrounding brain (Fig. 18). Observation of acute or subacute blood byproducts outside the hemosiderin rim suggests recent hemorrhage.

Traditionally, CMs are thought to be angiographically occult, but a mild capillary blush or venous pooling may be demonstrated on angiography in a small group of patients [109].

Brain tumors

Some type of bleeding is associated with 10% of metastatic and 5% of primary brain tumors. Hemorrhage is responsible for the initial clinical presentation in one third of these patients [85,110–112]. Bronchogenic carcinoma metastases are the most commonly encountered hemorrhagic tumors, although metastases from choriocarcinoma, melanoma, and renal cell carcinoma have a higher intrinsic tendency to bleed [113]. Glioblastoma multiforme is the most common primary neoplasm associated with hemorrhage [112]. Intratumoral hemorrhage occurs because of structural abnormalities of the vessels, resulting from either immature neovascularization of the tumor, direct infiltration of the blood vessel by the neoplastic cells, or necrosis of the vessel wall by tumor compression [112–114]. The coagulopathy not infrequently seen in this patient population may predispose or aggravate bleeding.

The pattern of hemorrhage in association with the underlying brain tumor is often slightly different from the more common causes of spontaneous ICH and can be readily identified on CT and MRI [115]. Typically, hematoma occupies a portion of the tumor, and careful evaluation of the pre- and postcontrast images reveals an eccentric enhancing rim or nodular mass (Figs. 19 and 20). Surrounding edema demonstrates a typical, finger-like, vasogenic edema pattern in most hemorrhagic tumors, whereas halo-like edema is more commonly seen in acute hematomas. Tumor-related hemorrhage shows much more heterogeneity than in other ICH caused by a nonhemorrhagic tumor. In addition, MRI offers a unique advantage in identifying blood byproducts of different ages, which, when present, suggest repeated hemorrhage into an underlying lesion. Atlas et al [116] reported

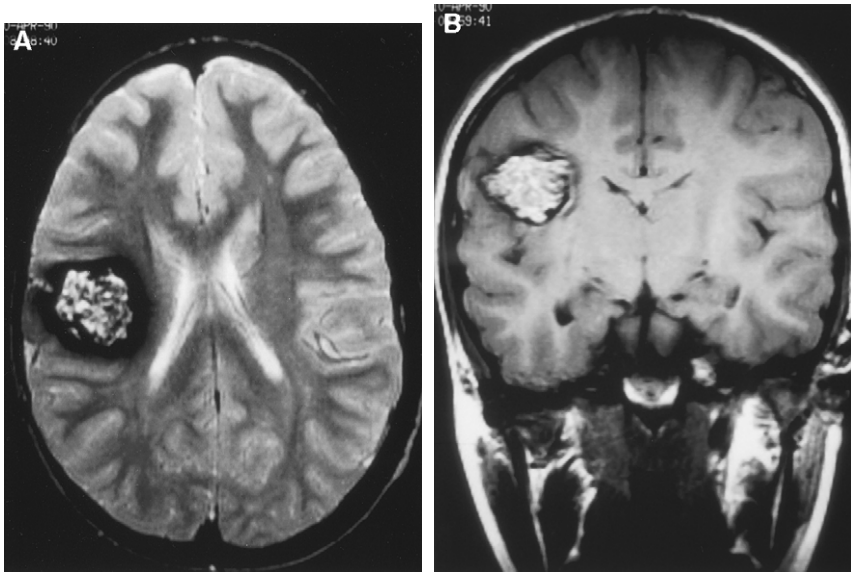

Fig. 16. Typical appearance of cavernous malformation on T2-weighted (A) and T1-weighted (B) images.

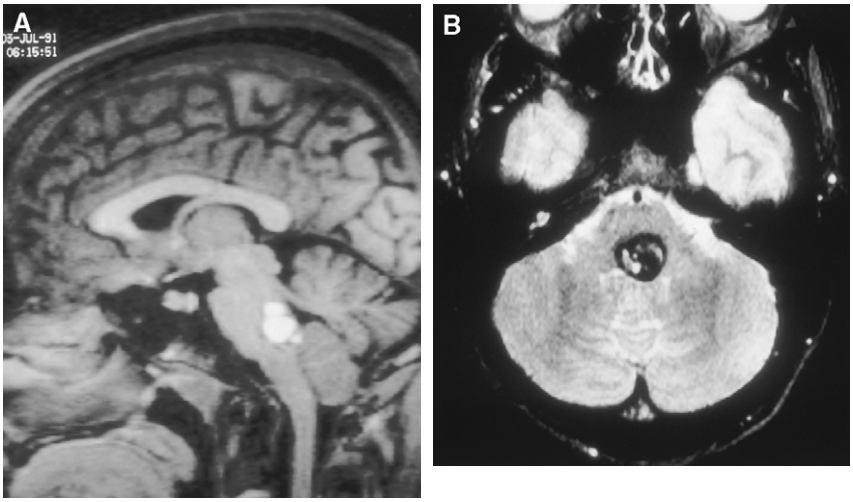

Fig. 17. Cavernous malformation in the pontine tegmentum. (A) T1-weighted image. (B) T2-weighted image.

that the hypointense rim seen on T2WIs in nontumoral bleeds was irregular or absent in intratumoral hemorrhages.

Rarely, when hemorrhage fills the entire tumor cavity, identification of the underlying tumor may be impossible on the initial imaging studies. This emphasizes the need and importance of follow-up MRI examinations. Resolving hematoma may unmask the tumor on follow-up studies. Differences in the temporal evolution of hemorrhage may be a clue to a preexisting lesion. Intratumoral hemorrhage evolves more slowly than nontumoral ICH [116].

Occasionally, a CM with acute hemorrhage may mimic intratumoral hemorrhage. The presence of a regularly thick hemosiderin rim, additional hemorrhagic lesions with chronic blood byproducts, and lack of enhancement are helpful findings in differentiating CM from tumor.

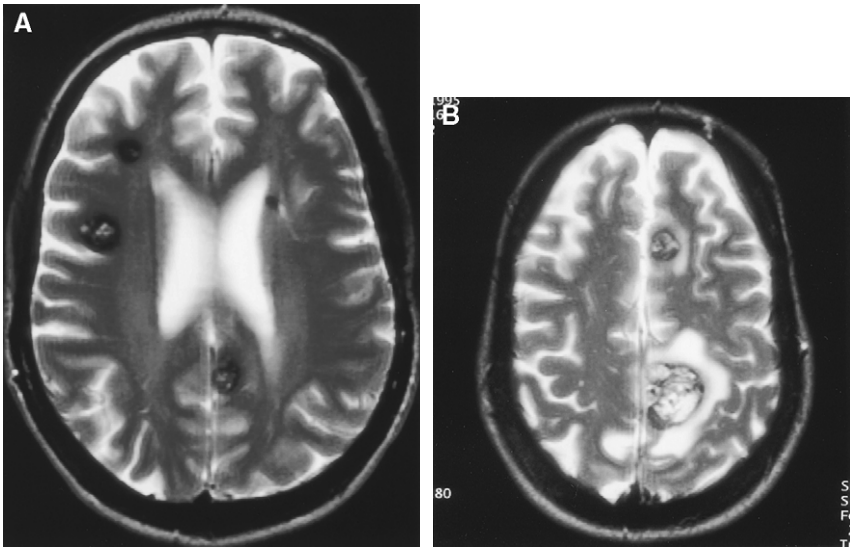

Fig. 18. (A,B) Multiple cavernous malformations (CMs). (B) Increased signal surrounding the left mesial parietal CM reflects recent hemorrhage.

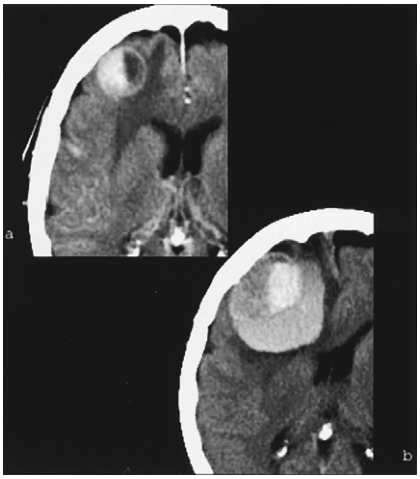

Fig. 19. Hemorrhagic metastasis. (a) Contrast-enhanced CT shows a prominently enhancing mass with a cystic component in the right frontal lobe. Three days later, the patient presented with headache and lethargy. Unenhanced CT demonstrates acute hemorrhage into the existing metastasis. The relatively decreased attenuation at the periphery of the hematoma is caused by dilution of blood byproducts with cyst contents.

Pituitary apoplexy is a clinical syndrome characterized by sudden-onset headache, vomiting, visual impairment, and meningismus caused by rapid enlargement of a pituitary adenoma as a result of hemorrhagic infarction of the tumor. Identification of blood byproducts and infarction within a pituitary adenoma is not uncommon on imaging studies and in pathology specimens, but this should not be termed *apoplexy* if the clinical symptoms are lacking. Headache is almost invariably present, and some degree of visual impairment is common. Hematoma is usually confined to the adenoma, which typically extends to the suprasellar cistern (Fig. 21). Rupture into the subarachnoid space is rare. Hypertension seems to be an important predisposing factor [117,118]. Early surgery provides complete restoration of the visual acuity in most patients. Some patients may require long-term hormone supplementation.

CT demonstrates a hyperdense mass in the sella and suprasellar cistern, but its sensitivity is around 20%. MRI is approximately 90% sensitive for the detection of this condition. Depending on the time of the imaging, MRI demonstrates either decreased T2 signal (first few days) or increased T1 signal (after 3 days) within the mass (Fig. 22). Hemosiderin deposition is not seen around the old hematomas, probably because of an absent blood–brain barrier and effective iron turnover.

Fig. 20. Prostate carcinoma metastasis. Hemorrhagic extra-axial metastasis from prostate carcinoma. Note the relatively low-attenuation mass and high-attenuation acute bleed in the mesial aspect of the mass.

Intracerebral hemorrhage associated with coagulopathy

Coagulation is regulated by several integrated complex biochemical mechanisms, and abnormalities induced by a variety of factors can cause or aggravate ICH. In the era of aggressive medical management of variety of disorders, including

Fig. 21. Pituitary apoplexy. Acute hemorrhage into a macroadenoma, which fills the suprasellar cistern.

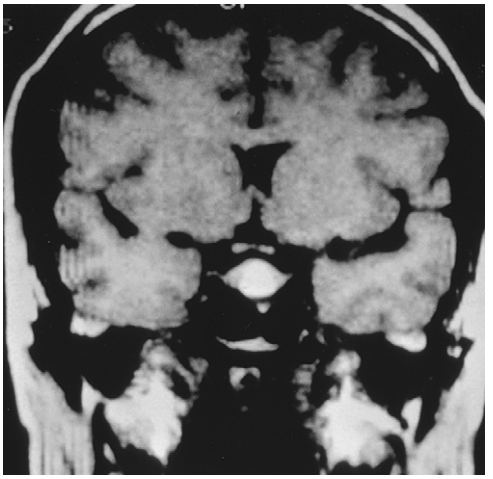

Fig. 22. Pituitary apoplexy. T1-weighted image obtained 4 days after the acute clinical presentation shows increased signal within a pituitary mass indicating subacute hemorrhage.

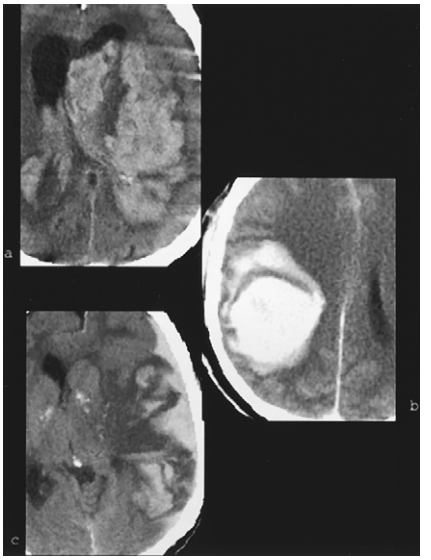

Fig. 23. Large left hemispheric hematoma involving the deep gray matter nuclei and white matter with intraventricular extension. The patient was on coumadin because of atrial fibrillation. (a) Relatively decreased attenuation of the hematoma is likely secondary to lack of clot formation. (b) Large lobar hematoma in a patient who received thrombolytic therapy because of myocardial infarction. Intraparenchymal, subdural, and subarachnoid hemorrhage with a blood–fluid level in a heparinized patient. (c) The blood–fluid level and involvement of different compartments are highly suggestive of underlying coagulopathy.

cerebral and myocardial infarction, ICH caused by anticoagulant, antiplatelet, and thrombolytic use is increasing [119].

The pattern of hemorrhage caused by coagulopathy is generally different than the pattern seen with more common causes of ICH. Coagulopathy-related ICH results in larger hematomas and is more commonly lobar in location [119–122]. There is less edema around the coagulopathy-related ICH [120]. Involvement of different intracranial compartments at the same time, unusual location of the hematoma, and multiple hematomas should prompt an investigation for an underlying coagulopathy. The presence of blood–fluid levels in the hematoma is a fairly specific sign of underlying coagulopathy (Fig. 23) [34].

Hemorrhagic transformation of an embolic bland infarct is a common occurrence and is usually not associated with neurologic deterioration (Fig. 24). Parenchymal hemorrhage into an infarcted area, however, is generally recognized as a worsening in the neurologic status of the patient (Fig. 25). The risk of parenchymal hematoma is greater with intra-arterial or intravenous administration of thrombolytics [123,124].

Drug abuse

Illicit drug use has become a major etiologic factor for ICH, particularly in young populations in recent decades [125,126]. Cocaine is one of the most popular abused drugs and is clearly associated with increased risk of ICH. Acting as a postsynaptic reuptake inhibitor, cocaine prolongs the effects of norepinephrine and possibly serotonin, which are potent sympathomimetic agents. More than 90% of the cocaine-induced ICH and/or subarachnoid hemorrhage (SAH) occurs during or a few hours after its use [127,128]. A sudden and sharp increase in blood pressure is probably the most important mechanism by which cocaine induces ICH. Up to 50% of cocaine-related ICH denotes an underlying lesion, such as an aneurysm or AVM [125,127,128]. The location of ICH associated with cocaine use but without underlying vascular abnormalities resembles that of hypertensive ICH. Because of the high incidence of underlying vascular abnormalities, a cerebral angiogram should be a part of the evaluation in these patients when the location of the hematoma is unusual for hypertensive ICH or when there is SAH.

Cocaine-induced vasculitis is a controversial issue [129,130]. Autopsy studies demonstrate that

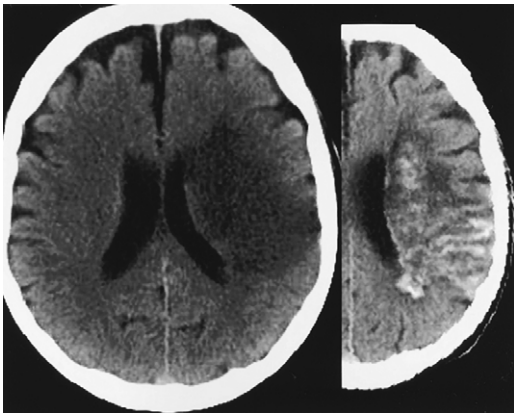

Fig. 24. Hemorrhagic transformation. Left frontoparietal acute infarct with follow-up study showing hemorrhagic transformation. No neurologic decline caused by hemorrhage was noted.

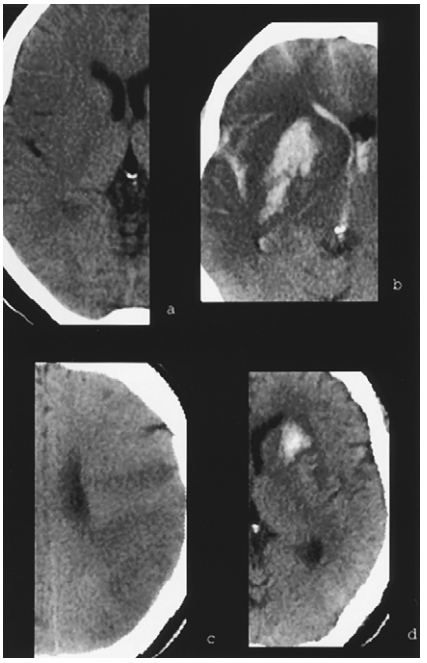

Fig. 25. Hemorrhagic infarct. (a) Right middle cerebral artery (MCA) territory acute infarct. (b) Putaminal hemorrhage identified on the next day was associated with neurologic deterioration. (d) In another patient with a clinical left MCA territory infarct, CT showed a left putaminal hematoma but no sign of an infarct. Follow-up study shows a frontoparietal infarct.

vasculitis is rare among the patients who died of cocaine-related ICH. Recently, animal studies showed that chronic exposure to cocaine increases the endothelial permeability, monocyte migration across the blood–brain barrier, and expression of cellular adhesion molecules and inflammatory cytokines, suggesting a potential pathophysiologic mechanism for the development of vasculitis [131,132]. It is not clear to what extent vasculitis plays a role in the development of ICH.

Hemorrhagic infarcts and unreported trauma are the other causes of cocaine-related ICH.

Other illicit drugs associated with ICH include amphetamines, phenylpropanolamine, phencyclidine, ephedrine, and pseudoephedrine. The primary mechanism of ICH is hypertensive bleeding, although amphetamines, ephedrine, and phenylpropanolamine have been known to produce vasculitis [120,133,134].

Miscellaneous

Cerebral venous occlusive disease may result in ICH, which is usually lobar in location, predominantly involving the subcortical white matter. The temporal lobe is the most common site (Fig. 26). The severity of parenchymal changes correlates well with the degree of venous sinus obstruction [135]. The presence of hematoma indicates markedly elevated venous pressure, which is invariably associated with diffuse cerebral swelling and T2-weighted signal abnormalities in the subcortical white matter [136].

ICH caused by rupture of infectious aneurysms (IAs) is generally a devastating event. Most of these aneurysms develop in the setting of bacterial endocarditis. Multiple foci of hemorrhage are common. Contrast-enhanced imaging studies may demonstrate small round areas of abnormal parenchymal enhancement remote from the hemorrhage, presumably representing the parenchymal reaction to additional IAs. Intra-arterial digital subtraction angiography remains the diagnostic test of choice mainly because of the peripheral location of these usually small aneurysms, which makes magnetic resonance angiography ineffective. It is not practical to obtain digital subtraction angiography on every patient with bacterial endocarditis, because 95% of these patients do not develop aneurysms. Therefore, a low index of suspicion is important in the diagnosis of IA. Intravenous antibiotic therapy is the cornerstone of the treatment. Early surgical/endovascular treatment may be life saving [137].

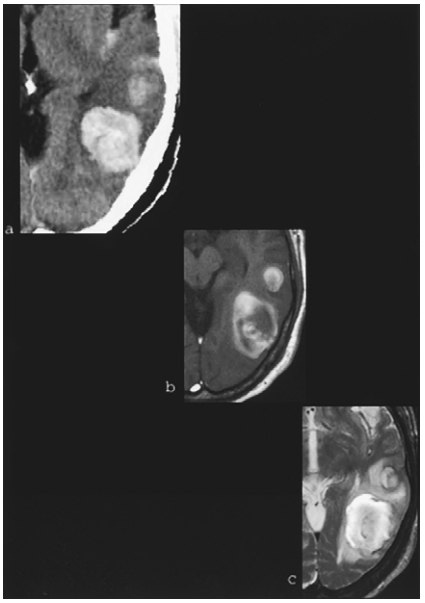

Fig. 26. Transverse sinus thrombosis. (a) Acute lobar hematoma on CT in the left temporal lobe (a). T1-weighted image (b) and T2-weighted image (T2WI) (c) obtained 8 days after ictus demonstrate high signal at the periphery of the hematoma caused by extracellular methemoglobin. Note the thin dark rim on the T2WI, which reflects hemosiderin.

Moyamoya disease is a rare cause of ICH. Progressive occlusion of the anterior circulation vessels produces small collateral channels that are subject to abnormal hemodynamic stress and prone to micropseudoaneurysm formation and hemorrhage.

A variety of infectious and granulomatous diseases of the meninges and brain can be associated with ICH [138]. Immune and nonimmune vasculitides may present with SAH or ICH.

References

[1] Broderick JP, Brott T, Tomsick T, Miller R, Huster G. Intracerebral hemorrhage more than twice as common as subarachnoid hemorrhage. J Neurosurg 1993;78:188–91.

[2] Felber S, Auer A, Wolf C, Schocke M, Golaszewski S, Amort B, et al. [MRI characteristics of spontaneous intracerebral hemorrhage]. Radiologe 1999; 39:838–46.

[3] Hartmann M, Jansen O, Deinsberger W, Vogel J, Sartor K. MRI of acute experimental intracerebral hematoma. Neurol Res 2000;22:512–6.

[4] Kuker W, Thiex R, Rohde I, Rohde V, Thron A. Experimental acute intracerebral hemorrhage. Value of MR sequences for a safe diagnosis at 1.5 and 0.5 T. Acta Radiol 2000;41:544–52.

[5] Linfante I, Llinas RH, Caplan LR, Warach S. MRI features of intracerebral hemorrhage within 2 hours from symptom onset. Stroke 1999;30: 2263–7.

[6] Patel MR, Edelman RR, Warach S. Detection of hyperacute primary intraparenchymal hemorrhage by magnetic resonance imaging. Stroke 1996;27: 2321–4.

[7] Perl J, Tkach JA, Porras-Jimenez M, Lieber M, Obuchowski N, Ross JS, et al. Hemorrhage detected using MR imaging in the setting of acute stroke: an in vivo model. AJNR Am J Neuroradiol 1999;20:1863–70.

[8] Schellinger PD, Jansen O, Fiebach JB, Hacke W, Sartor K. A standardized MRI stroke protocol: comparison with CT in hyperacute intracerebral hemorrhage. Stroke 1999;30:765–8.

[9] Dylewski DA, Demchuk AM, Morgenstern LB. Utility of magnetic resonance imaging in acute intracerebral hemorrhage. J Neuroimaging 2000; 10:78–83.

[10] Kirkpatrick JBHA. Pathophysiology of ICH. Neuroimaging Clin North Am 1992;2:11–23.

[11] Dickerson REGI. Hemoglobin. Structure, function, evolution and pathology1983Menlo Park: Benjamin-Cummings. p. 1–60.

[12] Bradley WGJ. Hemorrhage and vascular abnormalities. In: Bradley WGJ, Bydder GM, editors. MRI atlas of the brain. London: Martin Dunita Ltd; 1990. p. 201–64.

[13] Bradley WGJ. MR appearance of hemorrhage in the brain. Radiology 1993;189:15–26.

[14] Kelley WMJB. Understanding ICH. A practical approach. MRI Decisions 1993;7:9–15.

[15] Joseph PM. Principles of image formation. In: Atlas SW, editor. Magnetic resonance imaging of the brain. 2nd edition. Philadelphia: Lippincott-Raven; 1996. p. 49–64.

[16] Wehrli FWMJ. The basis of MR contrast. In: Atlas SW, editor. Magnetic resonance imaging of the brain and spine. 2nd edition. Philadelphia: Lippincott-Raven; 1996. p. 29–48.

[17] Thulborn KR, Atlas SW. Intracranial hemorrhage. In: Atlas SW, editor. Magnetic resonance imaging of the brain and spine. 2nd edition. Philadelphia: Lippincott-Raven; 1996. p. 265–314.

[18] Bloembergen NPEPR. Relaxation effects in nuclear magnetic resonance absorption. Physics Review 1948;73:679–85.

[19] Gomori JM, Grossman RI, Goldberg HI, Zimmerman RA, Bilaniuk LT. Intracranial hematomas: imaging by high-field MR. Radiology 1985; 157:87–93.

[20] Clark RA, Watanabe AT, Bradley WGJ, Roberts JD. Acute hematomas: effects of deoxygenation, hematocrit, and fibrin-clot formation and retraction on T2 shortening. Radiology 1990;175:201–6.

[21] Seidenwurm D, Meng TK, Kowalski H, Weinreb JC, Kricheff II. Intracranial hemorrhagic lesions: evaluation with spin-echo and gradient-refocused MR imaging at 0.5 and 1.5 T. Radiology 1989; 172:189–94.
[22] Hackney DB, Atlas SW, Grossman RI, Gomori JM, Goldberg HI, Zimmerman RA, et al. Subacute intracranial hemorrhage: contribution of spin density to appearance on spin-echo MR images. Radiology 1987;165:199–202.
[23] Hardy PA, Kucharczyk W, Henkelman RM. Cause of signal loss in MR images of old hemorrhagic lesions. Radiology 1990;174:549–55.
[24] Thulborn KR, Sorensen AG, Kowall NW, McKee A, Lai A, McKinstry RC, et al. The role of ferritin and hemosiderin in the MR appearance of cerebral hemorrhage: a histopathologic biochemical study in rats. AJNR Am J Neuroradiol 1990;11:291–7.
[25] Gomori JM, Grossman RI, Goldberg HI, Hackney DB, Zimmerman RA, Bilaniuk LT. Occult cerebral vascular malformations: high-field MR imaging. Radiology 1986;158:707–13.
[26] Atlas SW, Mark AS, Grossman RI, Gomori JM. Intracranial hemorrhage: gradient-echo MR imaging at 1.5 T. Comparison with spin-echo imaging and clinical applications. Radiology 1988;168:803–7.
[27] Weingarten K, Filippi C, Zimmerman RD, Deck MD. Detection of hemorrhage in acute cerebral infarction. Evaluation with spin-echo and gradient-echo MRI. Clin Imaging 1994;18:43–55.
[28] Lin DDM, Filippi CG, Steever AB, Zimmerman RD. Detection of intracranial hemorrhage: comparison between gradient-echo images and b(0) images obtained from diffusion-weighted echo-planar sequences. AJNR Am J Neuroradiol 2001;22:1275–81.
[29] Liang L, Korogi Y, Sugahara T, Shigematsu Y, Okuda T, Ikushima I, et al. Detection of intracranial hemorrhage with susceptibility-weighted MR sequences. AJNR Am J Neuroradiol 1999; 20(8):1527–34.
[30] Jones KM, Mulkern RV, Mantello MT, Melki PS, Ahn SS, Barnes PD, et al. Brain hemorrhage: evaluation with fast spin-echo and conventional dual spin-echo images. Radiology 1992;182:53–8.
[31] El-Koussy M, Guzman R, Bassetti C, Stepper F, Barth A, Lovblad KO, et al. CT and MRI in acute hemorrhagic stroke. Cerebrovasc Dis 2000;10:480–2.
[32] Norman D, Price D, Boyd D, Fishman R, Newton TH. Quantitative aspects of computed tomography of the blood and cerebrospinal fluid. Radiology 1977;123:335–8.
[33] New PF, Aronow S. Attenuation measurements of whole blood and blood fractions in computed tomography. Radiology 1976;121:635–40.
[34] Pfleger MJ, Hardee EP, Contant CFJ, Hayman LA. Sensitivity and specificity of fluid-blood levels for coagulopathy in acute intracerebral hematomas. AJNR Am J Neuroradiol 1994;15:217–23.
[35] Weisberg LA. Computerized tomography in intracranial hemorrhage. Arch Neurol 1979;36:422–6.
[36] Zimmerman RD, Leeds NE, Naidich TP. Ring blush associated with intracerebral hematoma. Radiology 1977;122:707–11.
[37] Bergstrom M, Ericson K, Levander B, Svendsen P, Larsson S. Variation with time of the attenuation values of intracranial hematomas. J Comput Assist Tomogr 1977;1:57–63.
[38] Furlan AJ, Whisnant JP, Elveback LR. The decreasing incidence of primary intracerebral hemorrhage: a population study. Ann Neurol 1979;5: 367–73.
[39] Walker AE, Robins M, Weinfeld FD. The National Survey of Stroke. Clinical findings. Stroke 1981;12(Suppl 1):I13–44.
[40] Brott T, Thalinger K, Hertzberg V. Hypertension as a risk factor for spontaneous intracerebral hemorrhage. Stroke 1986;17:1078–83.
[41] Zhu XL, Chan MS, Poon WS. Spontaneous intracranial hemorrhage: which patients need diagnostic cerebral angiography? A prospective study of 206 cases and review of the literature. Stroke 1997; 28:1406–9.
[42] Gokaslan ZLNR. Intracranial hemorrhage in the hypertensive patient. Neuroimaging Clin North Am 1992;2:171–86.
[43] Broderick JP, Brott TG, Tomsick T, Barsan W, Spilker J. Ultra-early evaluation of intracerebral hemorrhage. J Neurosurg 1990;72:195–9.
[44] Brott T, Broderick J, Kothari R, Barsan W, Tomsick T, Sauerbeck L, et al. Early hemorrhage growth in patients with intracerebral hemorrhage. Stroke 1997;28:1–5.
[45] Fujii Y, Takeuchi S, Sasaki O, Minakawa T, Tanaka R. Multivariate analysis of predictors of hematoma enlargement in spontaneous intracerebral hemorrhage. Stroke 1998;29:1160–6.
[46] Fujii Y, Tanaka R, Takeuchi S, Koike T, Minakawa T, Sasaki O. Hematoma enlargement in spontaneous intracerebral hemorrhage. J Neurosurg 1994;80:51–7.
[47] Kazui S, Naritomi H, Yamamoto H, Sawada T, Yamaguchi T. Enlargement of spontaneous intracerebral hemorrhage. Incidence and time course. Stroke 1996;27:1783–7.
[48] Zazulia AR, Diringer MN, Derdeyn CP, Powers WJ. Progression of mass effect after intracerebral hemorrhage. Stroke 1999;30:1167–73.
[49] Suga S, Sato S, Yunoki K, Mihara B. Sequential change of brain edema by semiquantitative measurement on MRI in patients with hypertensive intracerebral hemorrhage. Acta Neurochir Suppl (Wien) 1994;60:564–7.
[50] Fazekas F, Kleinert R, Roob G, Kleinert G, Kapeller P, Schmidt R, et al. Histopathologic analysis of foci of signal loss on gradient-echo T2*-weighted MR images in patients with spontaneous intracerebral hemorrhage: evidence of

microangiopathy-related microbleeds. AJNR Am J Neuroradiol 1996;20:637–42.
[51] Offenbacher H, Fazekas F, Schmidt R, Koch M, Fazekas G, Kapeller P. MR of cerebral abnormalities concomitant with primary intracerebral hematomas. AJNR Am J Neuroradiol 1996;17: 573–8.
[52] Roob G, Schmidt R, Kapeller P, Lechner A, Hartung HP, Fazekas F. MRI evidence of past cerebral microbleeds in a healthy elderly population. Neurology 1999;52:991–4.
[53] Donauer E, Reif J, al-Khalaf B, Mengedoht EF, Faubert C. Intraventricular haemorrhage caused by aneurysms and angiomas. Acta Neurochir (Wien) 1993;122:23–31.
[54] Taheri SA, Wani MA, Lewko J. Intraventricular hemorrhage due to rupture of arteriovenous malformations. Zentralbl Neurochir 1990;51:201–5.
[55] Bilinska M, Swierkocka-Miastkowska M, Dobrzynska L. [Primary and secondary intraventricular hemorrhage—clinical analysis] Neurol Neurochir Pol 1999;32(Suppl 6):141–7.
[56] Marti-Fabregas J, Marti-Vilalta JL. [Primary ventricular hemorrhage] Rev Neurol (Paris) 2000;31: 187–91.
[57] Flemming KD, Wijdicks EF, Li H. Can we predict poor outcome at presentation in patients with lobar hemorrhage? Cerebrovasc Dis 1901;11:183–9.
[58] Kothari RU, Brott T, Broderick JP, Barsan WG, Sauerbeck LR, Zuccarello M, et al. The ABCs of measuring intracerebral hemorrhage volumes. Stroke 1996;27:1304–5.
[59] Diringer MN, Edwards DF, Zazulia AR. Hydrocephalus: a previously unrecognized predictor of poor outcome from supratentorial intracerebral hemorrhage. Stroke 1998;29:1352–7.
[60] Maeshima S, Truman G, Smith DS, Dohi N, Nakai K, Itakura T, et al. Apraxia and cerebral haemorrhage: the relationship between haematoma volume and prognosis. J Clin Neurosci 2000; 7:309–11.
[61] Tuhrim S, Horowitz DR, Sacher M, Godbold JH. Volume of ventricular blood is an important determinant of outcome in supratentorial intracerebral hemorrhage. Crit Care Med 1999;27:617–21.
[62] Gebel JM, Broderick JP. Intracerebral hemorrhage. Neurol Clin 2000;18:419–38.
[63] Hankey GJ, Hon C. Surgery for primary intracerebral hemorrhage: is it safe and effective? A systematic review of case series and randomized trials. Stroke 1997;28:2126–32.
[64] Juvela S, Heiskanen O, Poranen A, Valtonen S, Kuurne T, Kaste M, et al. The treatment of spontaneous intracerebral hemorrhage. A prospective randomized trial of surgical and conservative treatment. J Neurosurg 1989;70:755–8.
[65] Fernandes HM, Gregson B, Siddique S, Mendelow AD. Surgery in intracerebral hemorrhage. The uncertainty continues. Stroke 2000;31:2511–6.
[66] Zuccarello M, Brott T, Derex L, Kothari R, Sauerbeck L, Tew J, et al. Early surgical treatment for supratentorial intracerebral hemorrhage: a randomized feasibility study. Stroke 1999;30: 1833–9.
[67] Montes JM, Wong JH, Fayad PB, Awad IA. Stereotactic computed tomographic-guided aspiration and thrombolysis of intracerebral hematoma: protocol and preliminary experience. Stroke 2000;31:834–40.
[68] Miller DW, Barnett GH, Kormos DW, Steiner CP. Stereotactically guided thrombolysis of deep cerebral hemorrhage: preliminary results. Cleve Clin J Med 1993;60:321–4.
[69] Gregson BA, Mendelow AD, Fernandes H, Pearson AJ, Siddique MS. Surgery for intracerebral hemorrhage. Stroke 2000;31:791–2.
[70] Wagner KR, Xi G, Hua Y, Zuccarello M, de Courten-Myers GM, Broderick JP, et al. Ultraearly clot aspiration after lysis with tissue plasminogen activator in a porcine model of intracerebral hemorrhage: edema reduction and blood-brain barrier protection. J Neurosurg 1999;90:491–8.
[71] Qureshi AI, Ling GS, Khan J, Suri MF, Miskolczi L, Guterman LR, et al. Quantitative analysis of injured, necrotic, and apoptotic cells in a new experimental model of intracerebral hemorrhage. Crit Care Med 2001;29:152–7.
[72] Siddique MS, Fernandes HM, Arene NU, Wooldridge TD, Fenwick JD, Mendelow AD. Changes in cerebral blood flow as measured by HMPAO SPECT in patients following spontaneous intracerebral haemorrhage. Acta Neurochir Suppl (Wien) 2000;76:517–20.
[73] Shang MQ, Yu JP, Wang UD. [Changes of regional cerebral blood flow in patients with intracerebral hemorrhage by ^{133}xenon inhalation method]. Zhonghua Nei Ke Za Zhi 1990;29:491–3.
[74] Zazulia AR, Diringer MN, Videen TO, Adams RE, Yundt K, Aiyagari V, et al. Hypoperfusion without ischemia surrounding acute intracerebral hemorrhage. J Cereb Blood Flow Metab 2001;21: 804–10.
[75] Hall NC, Packard BA, Hall CL, de Courten-Myers G, Wagner KR. Protein oxidation and enzyme susceptibility in white and gray matter with in vitro oxidative stress: relevance to brain injury from intracerebral hemorrhage. Cell Mol Biol (Noisy-le-Grand) 2000;46:673–83.
[76] Carhuapoma JR, Wang PY, Beauchamp NJ, Keyl PM, Hanley DF, Barker PB. Diffusion-weighted MRI and proton MR spectroscopic imaging in the study of secondary neuronal injury after intracerebral hemorrhage. Stroke 2000;31:726–32.
[77] Yamada M. Cerebral amyloid angiopathy: an overview. Neuropathology 2000;20:8–22.
[78] Greenberg SM. Cerebral amyloid angiopathy: prospects for clinical diagnosis and treatment. Neurology 1998;51:690–4.

[79] O'Donnell HC, Rosand J, Knudsen KA, Furie KL, Segal AZ, Chiu RI, et al. Apolipoprotein E genotype and the risk of recurrent lobar intracerebral hemorrhage. N Engl J Med 2000;342: 240–5.
[80] Greenberg SM, Vonsattel JP. Diagnosis of cerebral amyloid angiopathy. Sensitivity and specificity of cortical biopsy. Stroke 1997;28:1418–22.
[81] McCarron MO, Nicoll JA. Recurrent hemorrhage in cerebral amyloid angiopathy. Neurology 1998; 51:924–5.
[82] Greenberg SM, Vonsattel JP, Stakes JW, Gruber M, Finklestein SP. The clinical spectrum of cerebral amyloid angiopathy: presentations without lobar hemorrhage. Neurology 1993;43: 2073–9.
[83] Greenberg SM, O'Donnell HC, Schaefer PW, Kraft E. MRI detection of new hemorrhages: potential marker of progression in cerebral amyloid angiopathy. Neurology 1999;53: 1135–8.
[84] Cipri S, Gambardella G, Campolo C, Mannino R, Consoli D. Unusual clinical presentation of cerebral-isolated sarcoidosis. Case report and review of the literature. J Neurosurg Sci 2000;44:140–4.
[85] Das A, Hochberg FH. Clinical presentation of intracranial metastases. Neurosurg Clin North Am 1996;7:377–91.
[86] Eritaia J, Wood SJ, Stuart GW, Bridle N, Dudgeon P, Maruff P, et al. An optimized method for estimating intracranial volume from magnetic resonance images. Magn Reson Med 2000;44: 973–7.
[87] Miller JH, Wardlaw JM, Lammie GA. Intracerebral haemorrhage and cerebral amyloid angiopathy: CT features with pathological correlation. Clin Radiol 1999;54:422–9.
[88] Spetzler RF, Hargraves RW, McCormick PW, Zabramski JM, Flom RA, Zimmerman RS. Relationship of perfusion pressure and size to risk of hemorrhage from arteriovenous malformations. J Neurosurg 1992;76:918–23.
[89] Brown RDJ, Wiebers DO, Forbes G, O'Fallon WM, Piepgras DG, Marsh WR, et al. The natural history of unruptured intracranial arteriovenous malformations. J Neurosurg 1988;68:352–7.
[90] Brown RDJ, Wiebers DO, Forbes GS. Unruptured intracranial aneurysms and arteriovenous malformations: frequency of intracranial hemorrhage and relationship of lesions. J Neurosurg 1990;73:859–63.
[91] Crawford PM, West CR, Chadwick DW, Shaw MD. Arteriovenous malformations of the brain: natural history in unoperated patients. J Neurol Neurosurg Psychiatry 1986;49:1–10.
[92] Marks MP, Lane B, Steinberg GK, Chang PJ. Hemorrhage in intracerebral arteriovenous malformations: angiographic determinants. Radiology 1990;176:807–13.
[93] Ondra SL, Troupp H, George ED, Schwab K. The natural history of symptomatic arteriovenous malformations of the brain: a 24-year follow-up assessment [see comments]. J Neurosurg 1990;73: 387–91.
[94] Wilkins RH. Natural history of intracranial vascular malformations: a review. Neurosurgery 1985;16:421–30.
[95] Maraire JN, Awad IA. Intracranial cavernous malformations: lesion behavior and management strategies. Neurosurgery 1995;37:591–605.
[96] Brunereau L, Labauge P, Tournier-Lasserve E, Laberge S, Levy C, Houtteville JP. Familial form of intracranial cavernous angioma: MR imaging findings in 51 families. French Society of Neurosurgery. Radiology 2000;214:209–16.
[97] Sahoo T, Goenaga-Diaz E, Serebriiskii IG, Thomas JW, Kotova E, Cuellar JG, et al. Computational and experimental analyses reveal previously undetected coding exons of the KRIT1 (CCM1) gene. Genomics 2001;71:123–6.
[98] Zhang J, Clatterbuck RE, Rigamonti D, Dietz HC. Cloning of the murine Krit1 cDNA reveals novel mammalian 5′ coding exons. Genomics 2000;70:392–5.
[99] Zhang J, Clatterbuck RE, Rigamonti D, Dietz HC. Mutations in KRIT1 in familial cerebral cavernous malformations. Neurosurgery 2000;46: 1272–7.
[100] Davenport WJ, Siegel AM, Dichgans J, Drigo P, Mammi I, Pereda P, et al. CCM1 gene mutations in families segregating cerebral cavernous malformations. Neurology 2001;56:540–3.
[101] Lucas M, Costa AF, Montori M, Solano F, Zayas MD, Izquierdo G. Germline mutations in the CCM1 gene, encoding Krit1, cause cerebral cavernous malformations. Ann Neurol 2001;49: 529–32.
[102] Awad IA, Robinson JRJ, Mohanty S, Estes ML. Mixed vascular malformations of the brain: clinical and pathogenetic considerations. Neurosurgery 1993;33:179–88.
[103] Sure U, Butz N, Schlegel J, Siegel AM, Wakat JP, Mennel HD, et al. Endothelial proliferation, neoangiogenesis, and potential de novo generation of cerebrovascular malformations. J Neurosurg 2001;94:972–7.
[104] Uranishi R, Baev NI, Ng PY, Kim JH, Awad IA. Expression of endothelial cell angiogenesis receptors in human cerebrovascular malformations. Neurosurgery 2001;48:359–67.
[105] Clatterbuck RE, Moriarity JL, Elmaci I, Lee RR, Breiter SN, Rigamonti D. Dynamic nature of cavernous malformations: a prospective magnetic resonance imaging study with volumetric analysis. J Neurosurg 2000;93:981–6.
[106] Del COJ, Kelly DLJ, Elster AD, Craven TE. An analysis of the natural history of cavernous angiomas. J Neurosurg 1991;75:702–8.

[107] Kattapong VJ, Hart BL, Davis LE. Familial cerebral cavernous angiomas: clinical and radiologic studies. Neurology 1995;45:492–7.
[108] Momoshima S, Shiga H, Yuasa Y, Higuchi N, Kawase T, Toya S. MR findings in extracerebral cavernous angiomas of the middle cranial fossa: report of two cases and review of the literature. AJNR Am J Neuroradiol 1991;12:756–60.
[109] Rabinov JD. Diagnostic imaging of angiographically occult vascular malformations. Neurosurg Clin North Am 1999;10:419–32.
[110] Barth H, Fritsch G, Haaks T. [Intracerebral hematoma as an acute manifestation of intracranial tumors] Nervenarzt 1994;65:854–8.
[111] Bitoh S, Hasegawa H, Ohtsuki H, Obashi J, Fujiwara M, Sakurai M. Cerebral neoplasms initially presenting with massive intracerebral hemorrhage. Surg Neurol 1984;22:57–62.
[112] Kondziolka D, Bernstein M, Resch L, Tator CH, Fleming JF, Vanderlinden RG, et al. Significance of hemorrhage into brain tumors: clinicopathological study. J Neurosurg 1987;67:852–7.
[113] Mandybur TI. Intracranial hemorrhage caused by metastatic tumors. Neurology 1977;27:650–5.
[114] Liwnicz BH, Wu SZ, Tew JMJ. The relationship between the capillary structure and hemorrhage in gliomas. J Neurosurg 1987;66:536–41.
[115] Barkovich AJ, Atlas SW. Magnetic resonance imaging of intracranial hemorrhage. Radiol Clin North Am 1988;26:801–20.
[116] Atlas SW, Grossman RI, Gomori JM, Hackney DB, Goldberg HI, Zimmerman RA, et al. Hemorrhagic intracranial malignant neoplasms: spin-echo MR imaging. Radiology 1987;164:71–7.
[117] Biousse V, Newman NJ, Oyesiku NM. Precipitating factors in pituitary apoplexy. J Neurol Neurosurg Psychiatry 2001;71:542–5.
[118] Randeva HS, Schoebel J, Byrne J, Esiri M, Adams CB, Wass JA. Classical pituitary apoplexy: clinical features, management and outcome. Clin Endocrinol (Oxf) 1999;51:181–8.
[119] Franke CL, de Jonge J, van Swieten JC, Op dCA, van Gijn J. Intracerebral hematomas during anticoagulant treatment. Stroke 1990;21:726–30.
[120] Gebel JM, Brott TG, Sila CA, Tomsick TA, Jauch E, Salisbury S, et al. Decreased perihematomal edema in thrombolysis-related intracerebral hemorrhage compared with spontaneous intracerebral hemorrhage. Stroke 2000;31:596–600.
[121] Hart RG, Boop BS, Anderson DC. Oral anticoagulants and intracranial hemorrhage. Facts and hypotheses. Stroke 1995;26:1471–7.
[122] Neau JP, Couderq C, Ingrand P, Blanchon P, Gil R. Intracranial hemorrhage and oral anticoagulant treatment. Cerebrovasc Dis 2001;11:195–200.
[123] Anonymous. Tissue plasminogen activator for acute ischemic stroke. The National Institute of Neurological Disorders and Stroke rt-PA Stroke Study Group. N Engl J Med 1995;333:1581–7.
[124] Hacke W, Kaste M, Fieschi C, Toni D, Lesaffre E, von Kummer R, et al. Intravenous thrombolysis with recombinant tissue plasminogen activator for acute hemispheric stroke. The European Cooperative Acute Stroke Study (ECASS). JAMA 1995; 274:1017–25.
[125] McEvoy AW, Kitchen ND, Thomas DG. Intracerebral haemorrhage and drug abuse in young adults. Br J Neurosurg 2000;14:449–54.
[126] Qureshi AI, Mohammad Y, Suri MF, Braimah J, Janardhan V, Guterman LR, et al. Cocaine use and hypertension are major risk factors for intracerebral hemorrhage in young African Americans. Ethn Dis 2001;11:311–9.
[127] Fessler RD, Esshaki CM, Stankewitz RC, Johnson RR, Diaz FG. The neurovascular complications of cocaine. Surg Neurol 1997;47:339–45.
[128] Neiman J, Haapaniemi HM, Hillbom M. Neurological complications of drug abuse: pathophysiological mechanisms. Eur J Neurol 2000;7: 595–606.
[129] Aggarwal SK, Williams V, Levine SR, Cassin BJ, Garcia JH. Cocaine-associated intracranial hemorrhage: absence of vasculitis in 14 cases. Neurology 1996;46:1741–3.
[130] Kaye BR, Fainstat M. Cerebral vasculitis associated with cocaine abuse. JAMA 1987;258: 2104–6.
[131] Chang SL, Bersig J, Felix B, Fiala M, House SD. Chronic cocaine alters hemodynamics and leukocyte-endothelial interactions in rat mesenteric venules. Life Sci 2000;66:2357–69.
[132] Fiala M, Gan XH, Zhang L, House SD, Newton T, Graves MC, et al. Cocaine enhances monocyte migration across the blood-brain barrier. Cocaine's connection to AIDS dementia and vasculitis? Adv Exp Med Biol 1998;437:199–205.
[133] Janik P, Kwiecinski H, Opuchlik A, Dowzenko A. [Intracerebral hemorrhage following amphetamine use] Neurol Neurochir Pol 1998;32:1539–46.
[134] Perez JAJ, Arsura EL, Strategos S. Methamphetamine-related stroke: four cases. J Emerg Med 1999;17:469–71.
[135] Tsai FY, Wang AM, Matovich VB, Lavin M, Berberian B, Simonson TM, et al. MR staging of acute dural sinus thrombosis: correlation with venous pressure measurements and implications for treatment and prognosis. AJNR Am J Neuroradiol 1995;16:1021–9.
[136] Yuh WT, Simonson TM, Wang AM, Koci TM, Tali ET, Fisher DJ, et al. Venous sinus occlusive disease: MR findings. AJNR Am J Neuroradiol 1994;15:309–16.
[137] Clare CE, Barrow DL. Infectious intracranial aneurysms. Neurosurg Clin North Am 1992;3: 551–66.
[138] Roh JK, Kang DW. A case of tuberculosis meningitis complicated by intracerebral hemorrhage. Eur Neurol 1998;40:50–2.